

RESONANCES AND ENVELOPE INSTABILITY IN HIGH INTENSITY LINEAR ACCELERATORS

Dong-O Jeon[†], Ji-Ho Jang, Hyunchang Jin, Institute for Basic Science, Daejeon, S. Korea

Abstract

Understanding of space charge effects has grown and recent studies have led to the findings of space charge resonances in high intensity linear accelerators. Lately the sixth order resonance of high intensity linear accelerators was reported, along with the in-depth studies on the interplay of the fourth order resonance and the envelope instability. Experiment studies on space charge resonances were reported. This paper reviews the resonances of high intensity linear accelerators such as the $4\sigma = 360^\circ$, and the $6\sigma = 720^\circ$ resonances, along with the envelope instability.

INTRODUCTION

For high intensity beams, the envelope instability [1, 2] has been long known and the high intensity linac designers have kept $\sigma_0 < 90^\circ$ to avoid the envelope instability. However in 2009 researchers found that the space charge fourth order $4\sigma=360^\circ$ resonance was excited rather than the envelope instability [3] and was verified experimentally [4, 5]. Here $\sigma(\sigma_0)$ is the depressed (zero-current) phase advance per cell. These works led to further studies about the fourth order resonance and the envelope instability such as [6]. In 2015 it was reported that the envelope instability grows out of the mismatch induced by the fourth order resonance for a linear accelerator with a constant σ_0 lattice [7]. Recently a space charge sixth order $6\sigma=720^\circ$ resonance was found in the high intensity linear accelerators [8].

Space charge coupling resonances were measured in the linear accelerators [9-10, 5] and in the circular accelerators for example in [11].

Recent study showed that the envelope instability can be suppressed or excited after the development of the fourth order resonance by controlling the σ or σ_0 of the linac lattice [12].

This paper reviews the space charge resonances in high intensity linear accelerators; their simulation studies and the experiment studies, and the interplay of the fourth order resonance and the envelope instability.

THE FOURTH ORDER SPACE CHARGE RESONANCE

The space charge fourth order $4\sigma=360^\circ$ resonance was found and reported in 2009 [3]. It was observed that the fourth order resonance dominates over the envelope instability. Various studies were done to confirm that it was a resonance including the resonance crossing studies and the frequency analysis. It was shown that the resonance

takes effect only for $90^\circ - \Delta\sigma \leq \sigma \leq 90^\circ$ with a stopband $\Delta\sigma$. No fourth order resonance effect is found beyond 90° .

Figure 1 shows the four resonance islands of this resonance populated with beam particles. And Fig. 2 shows pronounced peaks at the tune of $1/4$ ($90^\circ/360^\circ$) for the $\sigma=85^\circ$ and $\sigma=75^\circ$ lattices. For the lattice with $\sigma=92^\circ$, one does not observe the peak at $1/4$. The lattices were designed to maintain a constant σ depressed phase advance per cell.

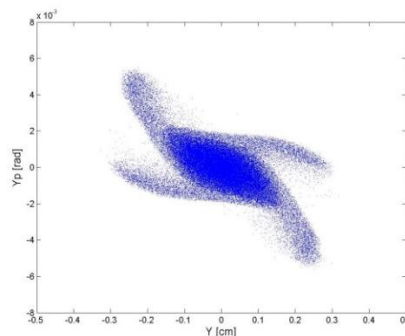


Figure 1: Beam distributions after the development of the fourth order resonance for the $\sigma = 85^\circ$ lattice (Courtesy of [3]).

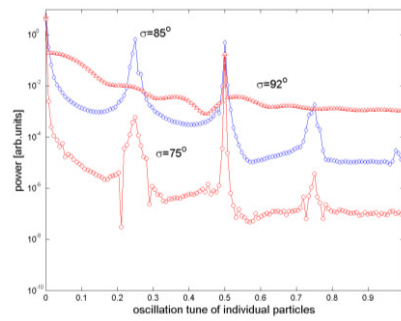


Figure 2: Plot of the FFT power spectrum of the rms beam size for the $\sigma=85^\circ$ and $\sigma=75^\circ$ lattices. One can see the pronounced peak at $1/4$ ($90^\circ/360^\circ$) due to the resonance. (Courtesy of [3])

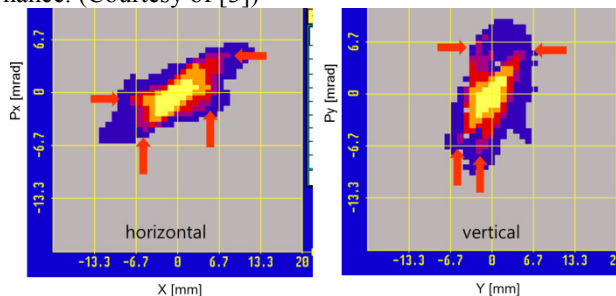


Figure 3: Measured x and y emittance for the lattice with $\sigma_0=100^\circ$ of the GSI UNILAC. Clear evidence of the fourth order resonance is observed. (Courtesy of [4])

[†] jeond@ibs.re.kr

This fourth order resonance was verified experimentally through the emittance measurement using the GSI UNILAC and reported in 2009 [4]. Four resonance islands are marked with red arrows in the emittance data shown in Fig. 3.

Another experiment was conducted recently to verify the fourth order resonance through the multiple beam profile measurements using the SNS linac [5]. Figure 4 shows the schematic layout of the CCL and the location of the wire-scanners used for the experiment. Beam profile measurements were done using all the wire-scanners in the CCL that follows the MEBT and the DTL.

Efforts were taken to minimize the halo of incoming beams by using the round beam MEBT optics [13] and by the matching experimentally between sections of the linac [14]. The beam profiles of the incoming beams were measured using the upstream wire-scanner and are shown in Fig. 5. The measured beam profiles are very close to Gaussian and no significant halos are observed. How the matching was done in the experiment is shown in Fig. 6 utilizing the upstream four wire-scanners. Solid dots are measured beam sizes.

Figure 7 shows the beam profiles from the simulation on the left and those from the experiment on the right at the wire-scanner WS304. The measured profiles agree well with the simulated profiles. The pronounced shoulders are due to the beam particles populating the resonance islands. Clear resonance shoulders are observed for the $\sigma=80^\circ$ lattice, while there are no resonance effects for the $\sigma=65^\circ$ lattice. The beam shoulders move toward the center while their intensity increase for the $\sigma=88.5^\circ$ lattice compared with the $\sigma=80^\circ$ lattice (bottom plots). This is also consistent with the simulation. Beam profiles from the other wire-scanners show a consistent pattern.

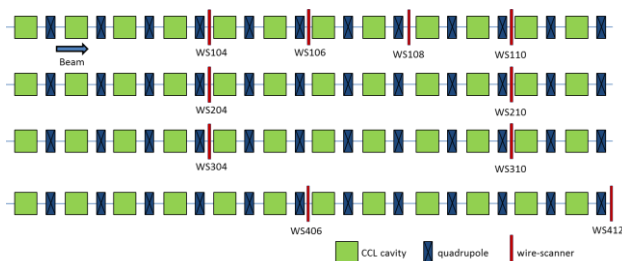


Figure 4: Schematic layout of the SNS CCL (Coupled Cavity Linac) and the location of wire-scanners used in the experiment. (Courtesy of [5])

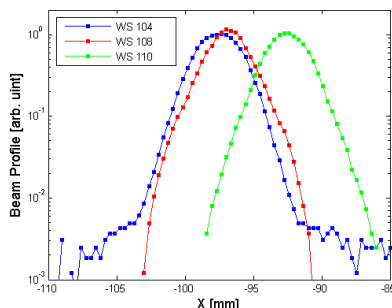


Figure 5: Measured x beam profiles of the incoming beam to the CCL using the upstream wire-scanner; WS104,

WS108 and WS110 in Fig. 4. Beam profiles indicate that there is no significant halo in the incoming beam. (Courtesy of [5])

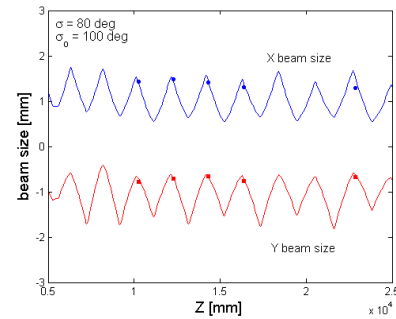


Figure 6: Plot showing how the matching was done. The beam envelope and measured beam sizes are shown.

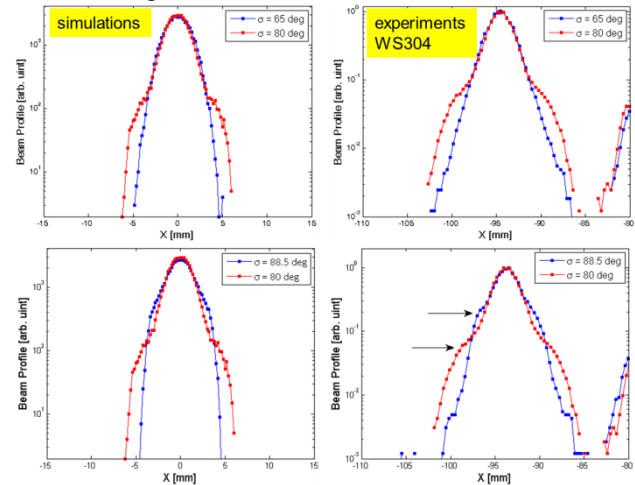


Figure 7: Beam profiles from the simulation on the left and those from the experiment on the right. The top plots show the beam profiles for the $\sigma=65^\circ$ and $\sigma=80^\circ$ lattices. The bottom plots show the beam profiles for the $\sigma=80^\circ$ and $\sigma=88.5^\circ$ lattices. The beam shoulders move toward the center while their intensity increase for the $\sigma=88.5^\circ$ lattice compared with the $\sigma=80^\circ$ lattice. The experiment results are consistent with the simulation.

THE SPACE CHARGE COUPLING RESONANCE

Space charge coupling resonances in linacs were extensively studied and verified in the experiment in the linear accelerators [9, 10, 5] and in the circular accelerators [11]. Recently the emittance exchange due to the coupling resonance was measured using the J-PARC linac [10].

The coupling resonance was experimentally measured using the SNS linac [5]. Figure 8 shows the phase advances for the “Coupled” and “Uncoupled” lattices and the corresponding emittances. Figure 9 shows the beam profiles for the two lattices obtained from the simulation at the wire-scanner WS310. It is shown that the space charge coupling resonance broadens beam profiles as a whole in both planes with little beam profile deformation.

The halo of incoming beam was minimized by the round beam MEBT optics and the matching. Figure 10 shows the measured beam profiles of the 38-mA beam in

log scale for the “Coupled” (in red) and the “Uncoupled” (in blue) lattices. The top left (right) plot shows the X (Y) beam profiles for the two cases obtained from the wire-scanner “WS310”. The bottom left (right) plot shows the X (Y) beam profiles from the wire-scanner “WS406”.

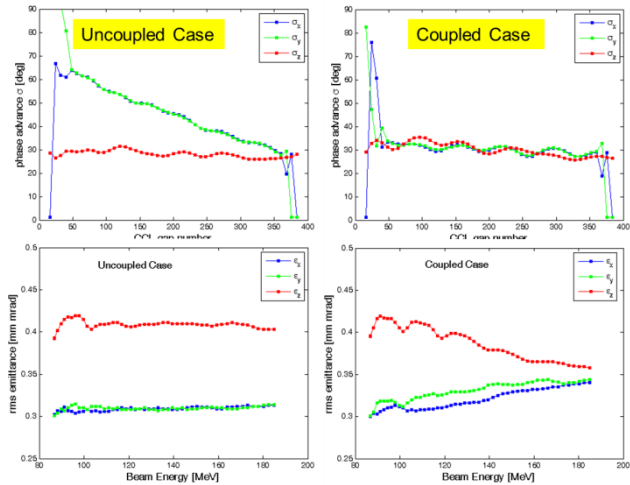


Figure 8: Plots of the phase advances s for the “uncoupled” lattice and the “coupled” lattice (top plots) and those of the corresponding emittances along the linac (bottom plots). For the “Coupled” case, the transverse and longitudinal phase advances almost overlap.

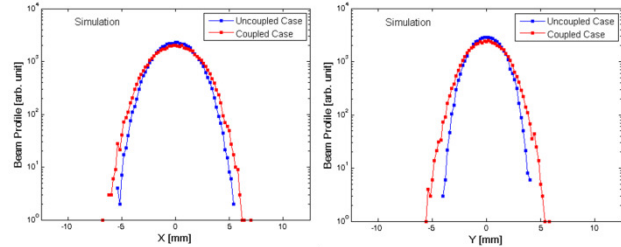


Figure 9: Simulated beam profiles in X and Y planes for the “Coupled” and the “Uncoupled” case at the wire-scanner WS310. One can notice that the space charge coupling resonance (in red) broadens beam profiles in both planes as a whole with little beam profile deformation.

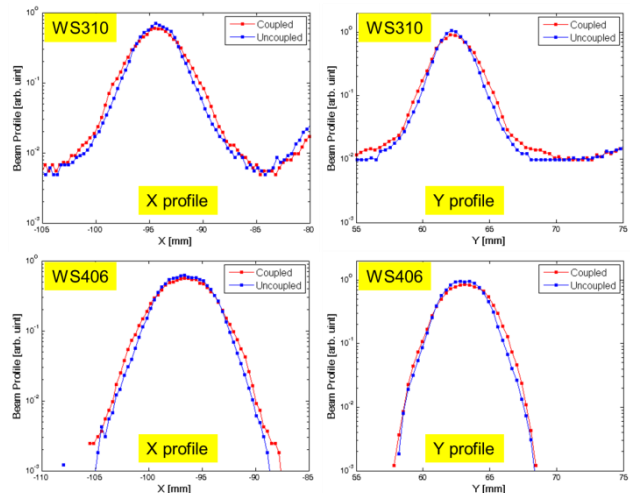


Figure 10: Plots of measured beam profiles from the wire-scanner WS310 and WS406 for the “Coupled” (in red)

case and the “Uncoupled” case (in blue). Consistent beam profile broadening is observed as predicted by the simulation. (Courtesy of [5])

Simulations and experiments show that the coupling resonance induces about 20% transverse emittance increase (in Fig. 8) and 10~20% beam profile broadening as a whole in both transverse planes at the downstream wire-scanners (in Fig. 9).

THE SIXTH ORDER SPACE CHARGE RESONANCE

The space charge sixth order $6\sigma=720^\circ$ resonance in high intensity linacs was found and reported in 2015 [8]. This resonance is observed for $120^\circ-\Delta\sigma \leq \sigma \leq 120^\circ$ with a stopband width $\Delta\sigma$. Transverse rms emittances vs the phase advance σ is shown in Fig. 11. The resonance effect disappears for $\sigma > 120^\circ$, which is a Hamiltonian property. Simulations show a clear emittance growth by this resonance in Fig. 11 and a characteristic six-fold resonance structure in phase space as shown in Fig. 12.

To verify that this is a resonance, a frequency analysis was conducted that shows a clear peak at $1/3$ ($120^\circ/360^\circ$) as shown in Fig. 13. A study was performed of crossing the resonance from above and from below the resonance, even though the results are not presented in this paper.

Canonical perturbation is carried out to show that this resonance arises through perturbation of strong $2\sigma=360^\circ$ (2:1) and $4\sigma=360^\circ$ (4:1) space charge resonances [8].

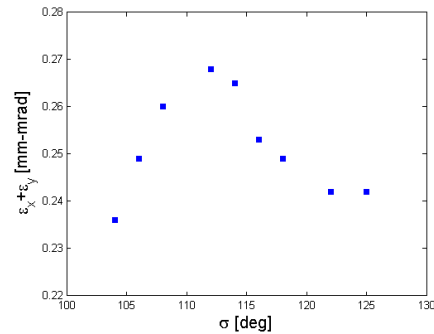


Figure 11: Plot of the transverse rms emittances vs. depressed phase advance per cell σ showing the emittance growth induced by the $6\sigma=720^\circ$ (or 6:2) space charge resonance of linacs. (Courtesy of [8])

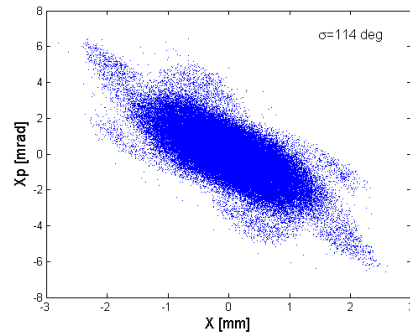


Figure 12: Plot of beam distribution for the lattice with $\sigma=114^\circ$ due to the $6\sigma=720^\circ$ resonance in Fig. 11. (Courtesy of [8])

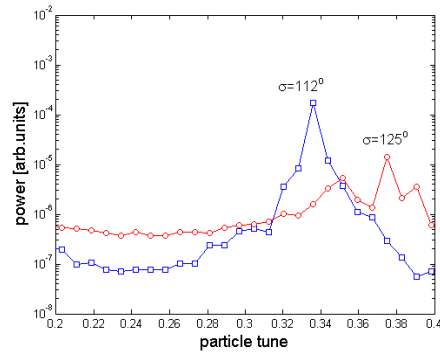


Figure 13: Plot of power spectrum of the frequency analysis on the rms beam size for the $\sigma=112^\circ$ and 125° lattices. A clear peak at $1/3$ ($120^\circ/360^\circ$) is observed for the $\sigma=112^\circ$ lattice and no peak is found for the $\sigma=125^\circ$ lattice beyond $\sigma=120^\circ$. (Courtesy of [8])

INTERPLAY OF FOURTH ORDER RESONANCE AND ENVELOPE INSTABILITY

Since the finding of the space charge fourth order $4\sigma = 360^\circ$ resonance [3], studies have been carried out to better understand the fourth order resonance and the envelope instability in high intensity linear accelerators [6, 7]. The questions remained unanswered under what conditions the envelope instability got excited or suppressed following the development of the fourth order resonance. Recent studies shed light on this subject [12] and are briefly presented in this paper. Well-matched Gaussian beams were used as input for the simulation.

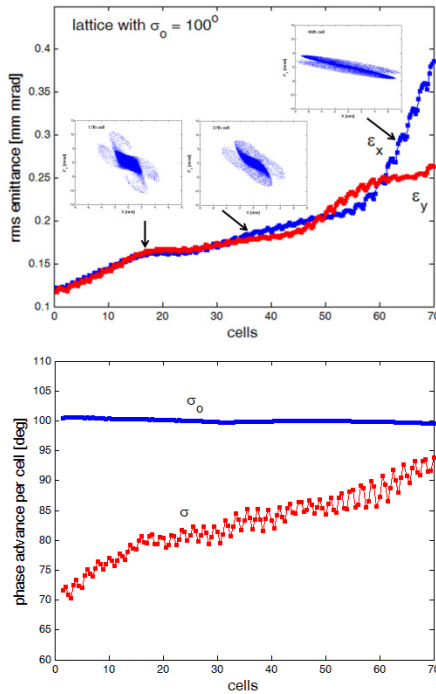


Figure 14: Plots of normalized rms emittances (the top plot) and the plot of σ_0 and σ in X plane for the linac lattice with $\sigma_0 \approx 100^\circ$. The fourth order resonance structure is observed at the 17th cell and the four-fold structure fades away outside the beam core at the 37th cell, as σ

increases approaching 90° and the resonance islands shrink. The emittance growth beyond the 50th cell is associated with the envelope instability that starts to take place when σ increases approaching 90° and the extent of the resonance shrinks. (Courtesy of [12])

Simulations suggest that the envelope instability is excited from the mismatch generated by the fourth order resonance, 1) when σ_0 is maintained approximately constant or increases along the linac with $\sigma_0 > 90^\circ$ and 2) when the extent of the fourth order resonance shrinks, as σ increases approaching 90° . Here $\sigma(\sigma_0)$ is the depressed (zero-current) phase advance per cell.

Figure 14 shows a case of the linac lattice with a constant σ_0 . In this case, σ increases as the beam is accelerated. Initially the fourth order resonance develops from the well-matched initial beam and later the envelope instability develops out of the mismatch generated by the fourth order resonance. The envelope instability is manifested when the extent of the resonance shrinks as σ increases approaching 90° .

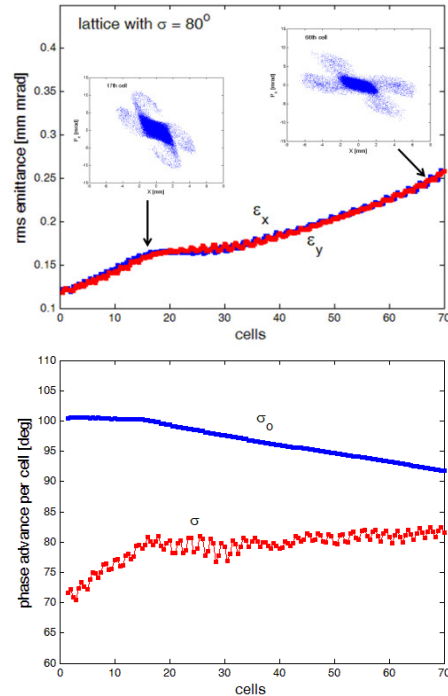


Figure 15: Plot of normalized rms emittances (the top plot) and the plot of σ_0 and σ in X plane. The downstream lattice is modified to keep $\sigma \approx 80^\circ$ from the 20th cell on. In this lattice with $\sigma \approx 80^\circ$ (from the 20th cell on), one does not observe the envelope instability. The fourth order resonance structure is formed by the 17th cell and persists throughout the linac and the envelope instability is not excited. Maintaining σ constant keeps the resonance islands outside the beam core, which seems to prevent the envelope instability. (Courtesy of [12])

On the other hand, when σ stays almost constant (maintaining the fourth order resonance) or when σ_0 decreases

and gets close to 90° (getting out of the envelope instability), the envelope instability is suppressed and the halo particles formed by the fourth order resonance preserves a four-fold structure in the phase space.

Maintaining σ constant keeps the resonance islands outside the beam core, which seems to prevent the envelope instability. In the lattice with $\sigma \approx 80^\circ$ (from the 20th cell on), one does not observe the envelope instability as in Fig. 15. The fourth order resonance structure is formed by the 17th cell and persists throughout the linac and the envelope instability is not excited.

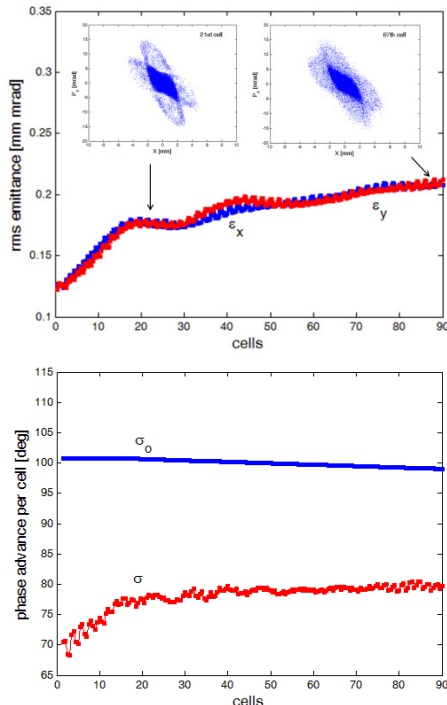


Figure 16: Plots of rms emittances (the top plot) and σ_0 , σ (the bottom plot) in X plane. The linac lattice is designed such that both σ_0 and σ remain almost constant by reducing the beam acceleration to zero, while the longitudinal focusing is maintained. The σ increases initially until the 16th cell due to the fourth order resonance and the redistribution of the beam, and then very slowly increases from 77° to 80° afterward. This is an ideal case to see whether the fourth order resonance dominates over the envelope instability or not. In this lattice the fourth order resonance persists and the envelope instability is not excited. (Courtesy of [12])

Now a linac lattice is designed such that both σ_0 and σ remain almost constant by reducing the beam acceleration to zero (setting synchronous phase to -90°), while the longitudinal focusing is maintained (see Fig. 16). The corresponding σ increases initially until the 16th cell due to the fourth order resonance and the redistribution of the beam, and then very slowly increases from 77° to 80° afterward. As an ideal case to test whether the fourth order resonance dominates over the envelope instability

or not, this case shows that the fourth order resonance persists and the envelope instability is not excited.

CONCLUSION

This paper reviews the space charge resonances in high intensity linear accelerators; their simulation studies and the experiments for the fourth order $4\sigma=360^\circ$ resonance and the space charge coupling resonances along with the space charge sixth order $6\sigma=720^\circ$ resonance.

Recent studies show that when σ stays almost constant (maintaining the fourth order resonance) or when σ_0 decreases and gets close to 90° (getting out of the envelope instability), the envelope instability is suppressed and the fourth order resonance preserves a four-fold structure in the phase space.

Simulations suggest that the envelope instability is excited from the mismatch generated by the fourth order resonance, 1) when σ_0 is maintained approximately constant or increases along the linac with $\sigma_0 > 90^\circ$ and 2) when the extent of the fourth order resonance shrinks, as σ increases approaching 90° .

ACKNOWLEDGEMENT

This work was supported by the Rare Isotope Science Project of the Institute for Basic Science funded by the Ministry of Science, ICT and Future Planning (MSIP) and the National Research Foundation (NRF) of the Republic of Korea under Contract 2013M7A1A1075764.

REFERENCES

- [1] I. Hofmann, L.J. Laslett, L. Smith, and I. Haber, Part. Accel. **13**, 145 (1983).
- [2] J. Struckmeier and M. Reiser, Part. Accel. **14**, 227 (1984).
- [3] D. Jeon, L. Groening, G. Franchetti, Phys. Rev. ST Accel. Beams **12**, 054204 (2009).
- [4] L. Groening et al., Phys. Rev. Lett. **102**, 234801 (2009).
- [5] Dong-O Jeon, Phys. Rev. Accel. Beams, **19**, 010101 (2016).
- [6] Chao Li and Ya Liang Zhao, Phys. Rev. ST Accel. Beams **17**, 124202 (2014).
- [7] I. Hofmann and O. Boine-Frankenheim, Phys. Rev. Lett. **115**, 204802 (2015).
- [8] Dong-O Jeon et al., Phys. Rev. Lett. **114**, 184802 (2015).
- [9] L. Groening et al., Phys. Rev. Lett. **103**, 224801 (2009).
- [10] C. Plostinar et al., Proc. of IPAC2013, Shanghai, China (2103), pp. 3966-3968.
- [11] G. Franchetti et al., Phys. Rev. ST Accel. Beams, **13**, 114203 (2010).
- [12] D. Jeon, J.H. Jang, H. Jin, Nucl. Instrum. Meth. A. **832** (2016) 43.
- [13] D. Jeon et al., Phys. Rev. ST Accel. Beams **5**, 094201 (2002).
- [14] D. Jeon et al., Nucl. Instrum. Meth. A **607** (2009) 51.